KINETICS, CATALYSIS, AND REACTION ENGINEERING

Decomposition of Formic Acid under Hydrothermal Conditions

Jianli Yu and Phillip E. Savage*

Department of Chemical Engineering, The University of Michigan, Ann Arbor, Michigan 48109-2136

The thermal decomposition of formic acid was studied in dilute aqueous solutions and in the absence of added oxygen at temperatures between 320 and 500 °C and pressures between 178 and 303 atm for residence times between 1.4 and 80 s. Under these conditions, the formic acid conversion ranged from 38% to 100%, and the major products were always CO_2 and H_2, which indicates that decarboxylation is the preferred reaction path for formic acid decomposition under hydrothermal conditions. CO also appeared as a product, which shows that a dehydration path is available, but the CO yield was always at least an order of magnitude lower than the yields of CO_2 and H_2. The kinetics of formic acid disappearance and product formation at temperatures above 320 °C are consistent with a reaction rate law that is first order in formic acid. The implications of the present results to the generally accepted molecular decomposition mechanism are discussed, as are the alternative free-radical, ionic, and surface-catalyzed reaction mechanisms proposed in the literature.

Introduction

Water at elevated temperatures and pressures continues to be explored as a chemical reaction medium (Savage et al., 1995; Katritzky et al., 1996; Mishra et al., 1995). One technological application that exploits oxidation reactions in water near its critical point (T_c = 374 °C, P_c = 218 atm) involves the safe conversion of organic wastes into innocuous compounds. When this chemical conversion occurs below the critical point of water, the technology is referred to as wet air oxidation. When the conversion occurs above the critical point of water, the technology is referred to as supercritical water oxidation. Regardless of the specific temperature and pressure of the aqueous reaction medium, however, carboxylic acids are frequently observed intermediate products from the hydrothermal oxidation of a wide variety of organic compounds and wastes (Thornton and Savage, 1990; Copa and Gitchel, 1989). As a consequence, a knowledge of the decomposition pathways, kinetics, and mechanisms for organic acids in high-temperature water is useful. In this paper we focus on the decomposition of the simplest organic acid, formic acid, in both sub- and supercritical water.

Although the literature provides experimental results for formic acid decomposition in the gas phase (Blake and Hinshelwood, 1960; Blake et al., 1971; Saito et al., 1984; Hsu et al., 1982) and formic acid oxidation in aqueous solutions (Wightman, 1981; Mishra et al., 1995), it provides much less information on the decomposition of formic acid in hot, aqueous solutions in the absence of added oxygen. Bjerre and Sørensen (1992) conducted two such experiments at 260 °C and in new and used reactors. The experiment in the used reactor resulted in a higher formic acid conversion, higher yields of CO_2 and H_2, and a lower yield of CO. In both reactors, however, the yield of CO_2 always exceeded that of CO. The authors attributed the differences in the results obtained from the two different reactors to the surface of the used reactor being rough and corroded and thereby influencing the reaction. Brill et al. (1996) reported preliminary results on the hydrothermal decomposition of formic acid up to 330 °C. They reported only the CO_2 concentration, and they observed that the temporal variation of the CO_2 concentration showed three distinct phases. The initial stage, which was not unimolecular, showed a monotonic increase in the CO_2 concentration with time. A second quiescent stage, where little conversion occurs, appeared next, and then a final explosive stage appeared, wherein decomposition is very rapid. These authors noted the similarity in these results to those reported by Falconer and Madix (1974) for the decomposition of formic acid on clean Ni(110) surfaces at 10^{-7} Torr and 100−125 °C and suggested that surface reactions were important in their hydrothermal reactor.

The present paper expands upon these two previous hydrothermal reaction studies and further broadens the field. We provide experimental data for the yields of formic acid and all of its major decomposition products as functions of time. Our experimental conditions include temperatures up to 500 °C, which is 170 °C higher than any previous hydrothermal studies. We explore the effects of temperature, pressure (or water density), and reactor surface/volume ratio and provide a quantitative kinetics analysis of formic acid decomposition under hydrothermal conditions.

Experimental Section

Formic acid was obtained from Aldrich in a nominal purity of 95−97% and used as received. An aqueous stock solution containing about 1000 ppm formic acid

* Corresponding author. E-mail: psavage@umich.edu. Phone: (313) 764-3386. Fax: (313) 763-0459.

S0888-5885(97)00182-6 CCC: $15.00
Published on Web 01/05/1998

was prepared with distilled, deionized, degassed water. This dilute aqueous solution served as the reactor feed, and it was loaded into a 1 gal pressure vessel blanketed with 500 psi helium before beginning an experiment.

Reactions were accomplished in a Hastelloy C-276 tubular flow reactor system, which has been previously described in detail (Thornton and Savage, 1990). The system comprises a nominal preheat section (1.08 mm i.d.) and a nominal reactor section joined to one another with a Hastelloy block that was fitted with a thermocouple. All reaction temperatures reported in this paper are the temperatures detected by this thermocouple. One of the reactors was 1 m long with 1.40 mm i.d., and a second reactor was 1.74 m long with 1.08 mm i.d. The tubular reactor system is immersed in a temperature-controlled (Techne TC-8D) fluidized bath (Techne SBL-2) of aluminum oxide particles. The nominal pressure and temperature were constant in the reactor section during each experiment. The formic acid solution was fed through the preheat line and then into the reactor tube by an Eldex high-pressure liquid chromatography pump. After leaving the heated reactor, the reactor effluent was rapidly cooled in a heat exchanger, depressurized, and then separated into gas and liquid phases at ambient conditions.

The vapor phase was directed to a 10-port Valco valve, which injected a known volume of gas (either 0.50 or 0.156 mL) into a Hewlett Packard Model 5890 series II gas chromatograph (GC) equipped with a thermal conductivity detector. Sample constituents were separated on a 10 ft. $\times$ $^1/_8$ in. o.d. stainless steel column packed with 100/120 mesh Supelco Carboseive S-II. Peak areas were calculated and reported by an HP 3392A integrator. The detector polarity was reversed before the hydrogen peak appeared so we could quantify the yield of hydrogen. The oven temperature was 35 °C for the first 7 min, and it then increased 16 °C/min until it reached 225 °C. Helium flowing at 20 mL/min served as the carrier gas. The flow rate of the vapor-phase reactor effluent was measured by using a soap-film flow meter.

The flow rate of the liquid-phase reactor effluent was determined by measuring the time required to fill a graduated cylinder of known volume. Samples of the liquid phase were collected and analyzed by a Waters high-performance liquid chromatograph (HPLC) equipped with a Supelco C610H gel column and operated isocratically with UV detection at 210 nm. The mobile phase was an aqueous solution of 0.1% H_3PO_4.

Both the GC and HPLC were calibrated by determining the detector response for sets of standards with known amounts of CO, CO_2, and H_2 (for the GC) and formic acid (for the HPLC). We typically made two independent measurements of the gas- and liquid-phase flow rates and compositions for each steady-state reaction condition. Molar yields of products were calculated as the molar flow rate of the product in the reactor effluent divided by the molar flow rate of reactant into the reactor. The molar yields calculated from the analytical results for the replicate samples always agreed to within a few percent. We assumed that the effluent gas and liquid streams are in equilibrium when these phases separate at ambient conditions, and we used Henry's law to calculate the amount of dissolved gases in the liquid phase. We also calculated the carbon balance as the percentage of carbon atoms in the feed that appear in quantified products in the reactor effluent.

The residence times reported for these experiments were calculated as the combined volume of the reactor and preheater sections divided by the volumetric flow rate of the fluid at the nominal reaction conditions less an estimated preheat time. The preheat time was taken to be constant for a given reaction temperature. It was calculated as the amount of time the flowing fluid spent in the preheater at the highest flow rate used in the experiments. We verified experimentally that this amount of time was sufficient to preheat the feed to the reaction temperature at the high flow rate. These preheat times were typically between 1 and 2 s. Given the weak sensitivity of the heat-transfer coefficient to the flow rate and the precise position in the preheater tubing (Holgate et al., 1992), we expect the preheat time to be only a weak function of the flow rate and hence roughly constant during a set of experiments at a fixed temperature. This approach provides a consistent basis for calculating the residence time.

Results

Tables 1 and 2 display the experimental conditions investigated and the results obtained in this study of the decomposition of formic acid under hydrothermal conditions. The results in Table 1 were obtained from a reactor with 1.40 mm i.d., whereas the results in Table 2 were obtained from a reactor with 1.08 mm i.d. In most cases, the results in Tables 1 and 2 are average values calculated from flow rate measurements and analyses of two, and at times four, different gas- and liquid-phase samples collected at the same nominal steady-state reaction conditions. We excluded from these tables results from experiments with carbon balances less than 85%. Only 8 of the roughly 150 data sets suffered from low carbon balances, and all eight of these data sets were from experiments run at low flow rates where the uncertainty in the gas-phase flow rate measurement is highest.

CO_2 is the major carbon-containing reaction product under all conditions studied. The yield of CO_2 is always at least an order of magnitude higher than the yield of CO. This high selectivity to CO_2 under hydrothermal conditions is consistent with the results of Brill et al. (1996) and Bjerre and Sørensen (1992). This result stands in contrast with previous gas-phase studies, however, where CO is the major product (Blake and Hinshelwood, 1960; Blake et al., 1971; Saito et al., 1984; Hsu et al., 1982). In a subsequent section of this paper we discuss reasons for this difference in the product spectrum for the hydrothermal and gas-phase decomposition.

If formic acid decomposes to form CO_2 as a major product, then stoichiometry demands that H_2 also be formed in equal yields. We were able to quantify the H_2 yields, and the results appear in Tables 1 and 2. The H_2 yield is always high and close to the value of the CO_2 yield. In fact, the CO_2/H_2 ratio is typically between 0.9 and 1.2, which shows that these two products appear in roughly equal yields. We estimate the uncertainty in the CO_2 and H_2 yields to be $\pm$10% and $\pm$15% of the reported values, respectively. These individual uncertainties lead to a relative uncertainty of 18% in the CO_2/H_2 ratio, which implies that nearly all of the experimental results possess a CO_2/H_2 ratio that includes the

Table 1. Formic Acid Decomposition at 250 atm and Different Temperatures

reaction temp (°C)	residence time (s)	formic acid conc. (mmol/L)	water conc. (mol/L)	formic acid conv. (%)	CO yield (%)	CO_2 yield (%)	H_2 yield (%)	carbon balance (%)
321	15.4	15.7	39.0	69	0.9	63	67	95
321	20.1	15.7	38.9	71	1.1	66	70	96
321	27.6	15.7	38.9	76	1.3	67	65	92
322	45.8	15.7	38.9	86	1.6	71	74	86
339	12.7	10.4	36.5	71	2.0	78	104	108
340	13.8	10.4	36.5	76	1.6	70	69	95
340	16.0	10.4	36.4	79	1.7	72	71	94
340	18.8	10.4	36.4	84	2.1	79	81	97
340	23.6	10.4	36.4	90	2.9	84	89	98
341	34.0	10.4	36.3	100	3.9	94	101	98
358	6.5	13.3	33.2	38	1.4	42	32	106
358	8.4	13.3	33.1	46	1.6	48	39	103
359	11.0	13.2	33.0	55	1.8	54	47	101
360	16.1	13.1	32.8	70	1.9	67	61	100
361	37.1	13.1	32.6	98	2.4	84	92	88
378	3.4	10.6	26.7	41	1.1	47	37	107
380	3.9	10.1	25.5	49	1.3	52	43	104
379	5.1	10.3	26.1	55	1.5	55	48	101
380	6.9	10.3	25.9	65	1.6	59	50	95
379	10.1	10.5	26.4	77	2.2	71	69	96
380	17.5	10.1	25.4	95	3.1	88	92	96
397	1.9	2.9	10.2	96	1.3	90	92	95
395	2.6	3.1	10.9	97	1.5	90	100	95
396	3.3	3.0	10.6	97	1.5	92	95	97
399	3.8	2.9	9.89	99	1.3	92	99	95
399	4.9	2.8	9.73	100	1.2	91	96	93
400	6.8	2.8	9.55	100	1.3	94	102	96
420	2.4	2.2	7.48	85	5.0	73	79	93
420	3.4	2.2	7.48	90	5.8	77	79	93
420	5.0	2.2	7.48	100	5.9	82	86	87
461	1.5	1.7	5.85	100	5.9	89	97	95
461	1.9	1.7	5.86	100	5.4	90	97	95
461	2.5	1.7	5.86	100	5.2	88	98	93
463	3.4	1.7	5.81	100	5.1	87	95	92
461	5.5	1.7	5.85	100	6.5	83	85	89
480	1.5	1.6	5.42	100	4.2	89	99	93
481	1.9	1.6	5.42	100	3.3	88	101	91
482	2.5	1.6	5.40	100	2.7	88	98	91
481	3.8	1.6	5.42	100	2.6	86	93	89
501	1.4	1.5	5.06	100	3.7	89	99	93
501	1.8	1.5	5.05	100	2.7	91	98	93
501	2.5	1.5	5.06	100	1.9	91	97	92
501	3.6	1.5	5.06	100	2.0	87	83	89

expected value of unity within their experimental uncertainties.

Figure 1 displays the temporal variations of the molar yields of the major carbon-containing products from formic acid decomposition at 250 atm and at 360, 380, and 420 °C. At all three temperatures, the formic acid yield steadily decreases with time while the CO_2 yield steadily increases. The yield of CO also increases with time, but the CO yield is much lower than the CO_2 yield. The monotonic trends in the product yields apparent in Figure 1 and in Tables 1 and 2 differ from the trends observed by Brill et al. (1996). As mentioned in the Introduction section, these investigators found that the CO_2 temporal profile exhibited three distinct regions. In the initial region the CO_2 yield increased monotonically, in the second region a "quiescent" period appeared wherein the CO_2 yield remained largely unchanged as the residence time increased, and in the final region an "explosive" increase in CO_2 production was observed. We found no need to invoke the existence of three different reaction stages to explain the formic acid decomposition data reported herein.

Reaction Kinetics

The analysis in this section focuses on the kinetics of formic acid disappearance. We first determine the reaction order and then the rate constant at several of the temperatures investigated.

The global reaction order, n, for formic acid disappearance can be determined by assessing the effect of the formic acid concentration, C, on the reaction rate.

$$\text{rate} = kC^n$$

To this end, we conducted a set of experiments at 360 °C and 250 atm wherein the concentration of formic acid in the reactor feed stream was varied by an order of magnitude but all other process variables (flow rate, temperature, pressure) remained unchanged. Each experiment provided the formic acid conversion, X, from which we calculated the pseudo-first-order rate constant, k', for formic acid disappearance as

$$k' = \frac{-\ln(1 - X)}{\tau}$$

Table 2. Formic Acid Decomposition at 380 °C and Different Pressures

reaction pressure (atm)	residence time (s)	formic acid conc. (mmol/L)	water conc. (mol/L)	formic acid conv. (%)	CO yield (%)	CO_2 yield (%)	H_2 yield (%)	carbon balance (%)
178	1.6	1.5	5.29	66	0.7	60	48	94
178	2.5	1.5	5.29	64	0.8	58	47	95
178	4.1	1.5	5.29	69	0.9	60	44	92
178	6.5	1.5	5.29	74	1.0	67	49	94
178	11.8	1.5	5.29	90	0.8	80	58	91
205	2.1	2.2	7.27	67	0.9	64	52	98
205	3.5	2.2	7.25	75	0.8	72	59	99
205	5.6	2.2	7.26	88	0.6	82	68	95
205	9.1	2.2	7.29	96	0.4	89	69	94
205	16.4	2.2	7.24	100	0.5	90	72	90
219	2.7	2.7	9.35	85	1.0	80	65	96
219	4.6	2.7	9.37	92	0.7	87	72	96
219	7.3	2.7	9.31	96	0.5	91	76	95
219	12.0	2.7	9.29	99	0.4	93	77	94
219	17.2	2.7	9.20	100	0.3	90	68	90
250	23.2	10.2	25.6	92	1.7	91	83	101
250	28.3	10.1	25.4	96	1.9	95	85	100
250	36.2	10.1	25.3	99	1.6	98	91	100
250	46.3	10.1	25.2	100	1.2	99	95	100
250	49.7	10.0	25.1	100	1.9	95	87	97
250	63.3	10.0	25.1	100	0.9	92	81	93
273	25.5	8.0	27.8	99	1.8	95	79	97
273	29.9	8.1	27.9	100	1.2	95	78	96
273	39.9	8.1	27.8	100	0.9	102	81	103
273	55.1	8.1	27.8	100	0.4	92	75	93
301	34.1	8.6	29.6	100	1.3	97	85	99
302	44.2	8.6	29.6	100	0.8	96	83	97
302	62.0	8.6	29.6	100	0.3	94	79	94
303	80.1	8.6	29.7	100	0.0	86	59	86

The pseudo-first-order rate constant is related to the formic acid concentration by

$$k' = kC_{\text{mean}}^{n-1}$$

so a log−log plot of these pseudo-first-order rate constants as a function of the mean formic acid concentration (C_{mean}) in the reactor during the experiment provides the global reaction order as 1 plus the slope of the best-fit line through the data. Figure 2 provides the log−log plot of the data, and the slope of the line that best fits the data is -0.06 ± 0.18. The uncertainty given here and elsewhere in this paper represents the 95% confidence interval about the reported value. Therefore, the global reaction order for formic acid decomposition under hydrothermal conditions is 0.94 ± 0.18. Given the uncertainty in the reaction order and its proximity to unity, we conclude that formic acid disappearance is adequately described by first-order kinetics under the conditions of the present experiments.

We can also use the results of the experiments in Figure 2 to obtain an estimate of the first-order rate constant at 360 °C. The seven experiments in Figure 2 gave rate constants that ranged from 0.10 to 0.15 s^{-1}, and the mean value was 0.127 ± 0.016 s^{-1}.

Having determined the reaction order and the rate constant at 360 °C, we next used the data in Tables 1 and 2 from experiments at 320, 340, 360, 380, and 420 °C to determine the first-order rate constant at each of these temperatures. Experiments at higher temperatures led to complete conversion even at the shortest residence times studied, so these high-temperature data are not useful for quantitative kinetics analysis. Linear regression of the data as $\ln(1/(1 - X))$ vs τ provided the rate constant as the slope of the line through the origin that best fit the experimental data.

Table 3, which lists these rate constants, shows that the rate constant at 250 atm increases as the temperature increases from 320 to 420 °C. Linear regression of these data as $\ln k$ vs $1/T$ (an Arrhenius plot) leads to Arrhenius parameters of $\log A$ (s^{-1}) = 6.2 and E = 20.5 kcal/mol. This preexponential factor is lower than transition state theory (Moore and Pearson, 1981) would lead one to expect for an elementary unimolecular reaction ($\log A \cong 13 \pm 1$). This low value can perhaps be rationalized, however, if there is a significant loss of entropy as the atoms in the reactant arrange themselves to form the activated complex. We note that ab initio quantum chemical calculations showed that the activated complex for the unimolecular gas-phase decomposition of formic acid to form CO_2 and H_2 involves a four-center transition state (Ruelle et al., 1986; Melius et al., 1990; Goddard et al., 1992; Francisco, 1992), as shown in Figure 3. This transition state is certainly more "ordered" than formic acid, so $\Delta S^{\ddagger}$ should be less than zero. According to these quantum chemical calculations, however, the activation energy for this decarboxylation path should be about 65−70 kcal/mol, which is much greater than the 20.5 kcal/mol we obtained from these experiments. Thus, these experimental Arrhenius parameters for the first-order rate constant for formic acid decomposition under hydrothermal conditions differ from those expected for a unimolecular elimination reaction in the gas phase based on quantum chemical calculations.

One possible reason for these differences is that the mechanism for the hydrothermal decomposition differs from the gas-phase mechanism and that water plays a role in the reaction. Ruelle et al. (1986) and Ruelle (1987) suggested that water is a catalyst for the decarboxylation reaction. Later, Melius et al. (1990) considered the potential catalytic effect of water on both the decarboxylation and dehydration paths. Illustrations

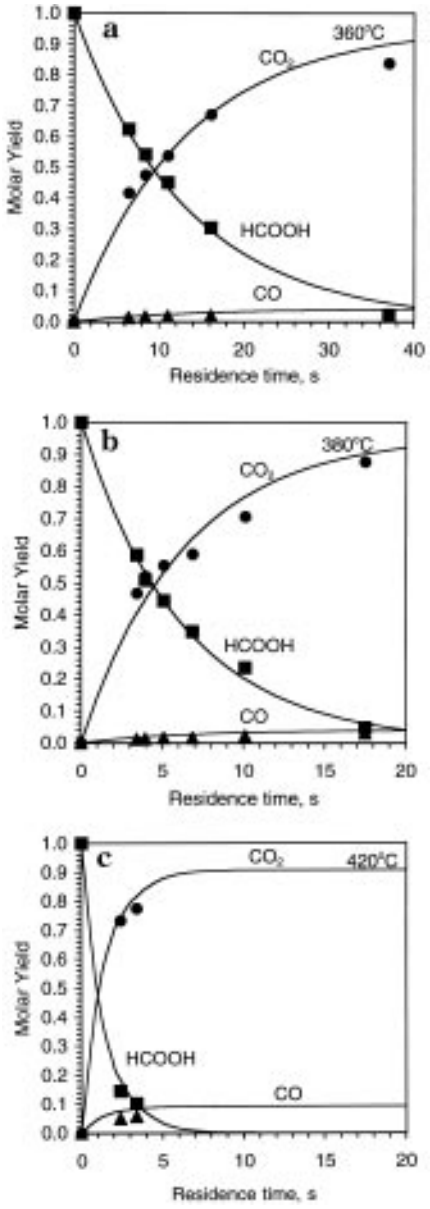

Figure 1. Temporal variation of product yields from formic acid decomposition at 250 atm (discrete points are experimental data; smooth curves are calculated from rate constants in Table 4): (a) 360 °C; (b) 380 °C; (c) 420 °C.

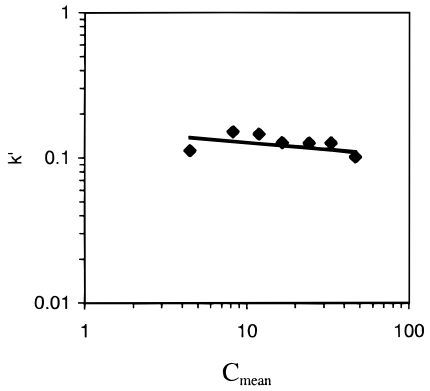

Figure 2. Effect of formic acid concentration on the first-order rate constant for formic acid disappearance at 360 °C and 250 atm.

of the relevant transition states for these water-catalyzed decomposition mechanisms appear in Figure 3. All of these quantum chemical calculations showed that the activation energy for a decarboxylation reaction

Table 3. Rate Constants for Formic Acid Disappearance under Hydrothermal Conditions

$-r_{HCOOH} = k[HCOOH]$ $\quad -r_{HCOOH} = k[HCOOH][H_2O]$

temp (°C)	pressure (atm)	k (1/s)	k (L/mol·s)	95% CI[a] (% of k)
320	250	0.050	0.0013	26
340	250	0.098	0.0027	3
360	250	0.127[b]	0.0038	13
360	250	0.097	0.0029	17
380	250	0.164	0.0063	8
420	250	0.719	0.096	24
380	178	0.216	0.041	36
380	205	0.366	0.050	13
380	219	0.430	0.046	20
380	250	0.116	0.0045	12
380	273	0.192	0.0069	n.d.[c]

[a] CI = confidence interval. [b] Determined from data in Figure 2. [c] n.d. = not determined because of insufficient data.

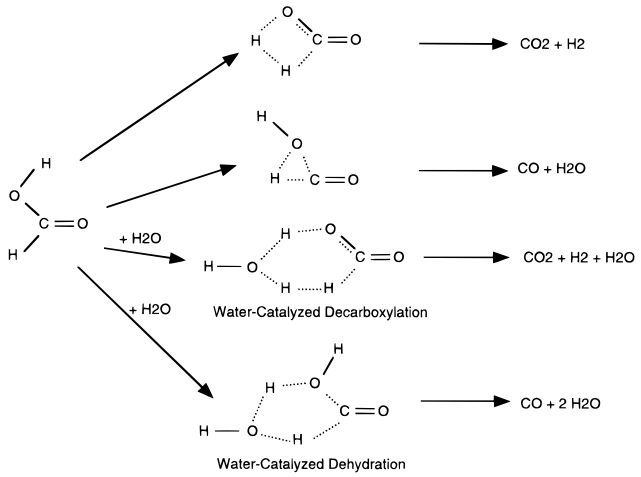

Figure 3. Illustration of molecular elimination mechanisms for formic acid decomposition.

that involved a water molecule in the transition state was about 20−25 kcal/mol lower than the activation energy of the competing unimolecular decomposition reactions. Therefore, we reassessed the experimental kinetics by exploring the possibility of the decomposition reaction being catalyzed by water and thereby being second order overall. The second-order rate constants, which also appear in Table 3, were calculated as the first-order rate constants divided by the water concentration (which was essentially constant) at reaction conditions. A linear regression of these second-order rate constants as ln k vs $1/T$ led to Arrhenius parameters of log A (L/mol·s) = 9.3 and E = 33.6 kcal/mol. This experimental activation energy of 33.6 ± 17.2 kcal/mol is similar to the activation energies of 48.7 kcal/mol, 45.3 and 47.9 kcal/mol, and 21.5 and 37.3 kcal/mol that Ruelle et al. (1986), Akiya and Savage (1998), and Melius et al. (1990) obtained from ab initio quantum chemical calculations for the water-catalyzed decarboxylation reaction. Moreover, the experimental preexponential factor is of the same order of magnitude as one would expect for a bimolecular reaction. Note, however, the uncertainty in the individual Arrhenius parameters is high because of the strong correlation between A and E, so one must exercise caution in assigning chemical significance to their numerical values.

To test further the effect of water on the decarboxylation reaction kinetics, we consider the sets of experi-

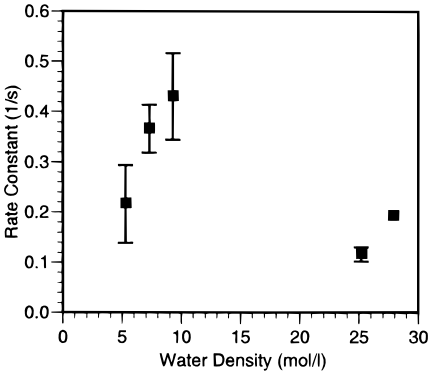

Figure 4. Effect of water density on first-order rate constants at 380 °C.

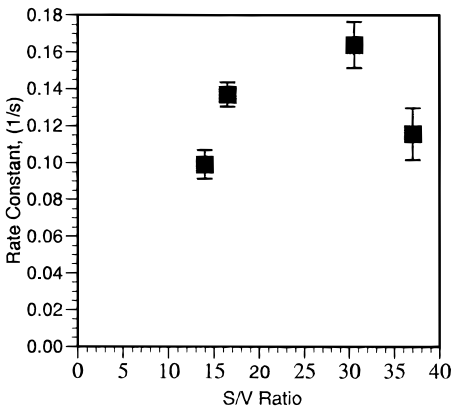

Figure 5. Effect of reactor surface/volume ratio on first-order rate constant at 380 °C and 250 atm.

ments conducted at a nominally constant temperature of 380 °C and at different pressures and hence different water densities. The results of these experiments appear in Table 2, the first-order rate constants at each pressure appear in Table 3, and the rate constant as a function of the water density at the reaction conditions appears in Figure 4. If the decarboxylation reaction occurs in a single elementary step that is catalyzed by a single water molecule, the kinetics of this reaction would be first order in water, which implies that a straight line through the data in Figure 4 would possess a slope of unity. The first three data points at the low water concentrations display precisely this trend, but the last two data points at the higher pressures clearly do not. The rate constant at the highest water density was calculated from a single experimental run, so it was not possible to calculate the 95% confidence interval for this rate constant. Given that the rate constant is an estimate based on a single point, however, we expect its uncertainty to exceed the uncertainties associated with the other rate constants in Figure 4.

A factor that complicates the proper discernment of the effect of pressure (or water density) on the decomposition kinetics is the possibility that the dominant decomposition mechanism might be density dependent. The calculations of Melius et al. (1990) revealed that, for the dehydration path, the unimolecular mechanism would be expected to be the fastest step at 700 K and 1 atm whereas a mechanism with one or two water molecules in the transition state would be expected to be the fastest step at 700 K and 300 atm. Even with this possible shift in mechanism as the density increases, however, one would expect the pseudo-first-order rate constant to increase with isothermal increases in the water density if the primary role of water is to catalyze the decomposition in a single elementary step. This expected monotonic increase is clearly not apparent in Figure 4.

Rice and co-workers (1996) at the Combustion Research Facility in Sandia National Laboratory have performed similar experiments to determine the effect of the water density on the kinetics of the water−gas shift reaction ($CO + H_2O = CO_2 + H_2$). Their experiments were motivated by Melius et al. (1990) proposing a formic acid intermediate for this reaction and, as noted above, predicting that high water densities would reduce the energy barriers and accelerate the reaction rate. The group at Sandia confirmed this prediction by observing that a 3-fold increase in the water density (from 9.4 to 30.8 mol/L) at 410 °C resulted in a 40-fold increase in the rate of CO disappearance. Our data in Figure 4 show, at most, a 4-fold difference in rate over roughly the same range of water densities. Integrating these two sets of data suggests that the rate of formation of formic acid from CO and H_2O is slow and strongly dependent on the water density, whereas the decomposition of formic acid to CO_2 and H_2 is much faster and the decomposition kinetics are much less sensitive to the water density.

The previous reports (Bjerre and Sørensen, 1992; Brill et al., 1996) on the hydrothermal decomposition of formic acid have either identified or intimated that the reactor surface might influence the reaction kinetics. We conducted a set of experiments at identical nominal reaction conditions (380 °C, 250 atm) but with reactors with different inner diameters and therefore different surface area to volume (S/V) ratios to explore the effect of the S/V ratio on the decomposition kinetics. The results from these experiments appear in Figure 5, which displays the first-order rate constant for formic acid disappearance as a function of the S/V ratio. The two data points at the higher S/V ratios correspond to the rate constants already reported in Table 3, and the two data points at the lower S/V ratios were obtained in a reactor with a larger inner diameter of 4.8 mm. In one experiment, a smaller Hastelloy tube was placed inside the 4.8 mm i.d. reactor to give a slightly higher S/V ratio than that of the empty reactor system itself. The results in Figure 5 show that decreasing the reactor S/V ratio had very little effect on the rate constant. This observation leads us to conclude that the kinetics data derived from the experimental data in Tables 1 and 2 are largely insensitive to the reactor S/V ratio (within the range of values explored experimentally). Thus, it appears that random error and not surface-catalyzed reactions is the main contributor to the 40% difference between the rate constants obtained from different reactors at 380 °C and 250 atm as reported in Table 3.

Reaction Network

Studies of formic acid decomposition in the gas phase (Blake and Hinshelwood, 1960; Blake et al., 1971; Saito et al., 1984; Hsu et al., 1982) showed that the main reaction was dehydration, which formed CO and H_2O, and that decarboxylation, which forms CO_2 and H_2, occurred to a lesser extent. The results in Tables 1 and 2, on the other hand, show that the main reaction under hydrothermal conditions is decarboxylation and that dehydration is much less important. Results from reactions both in the gas phase and in a hydrothermal

medium are consistent, however, in showing that at least two parallel paths are available for formic acid decomposition.

The discussion above suggests that the reaction network below can describe the main reaction paths for formic acid decomposition under hydrothermal conditions.

$$HCOOH \rightarrow CO_2 + H_2 \quad (1)$$

$$HCOOH \rightarrow CO + H_2O \quad (2)$$

This network includes parallel primary reactions for formic acid decomposition. The main route is reaction 1, which is the decarboxylation pathway. The minor route is reaction 2, which is the dehydration pathway.

As noted in the previous section, one possible explanation for the significant difference in the relative amounts of CO and CO_2 formed in the gas phase and in aqueous solution is that water enhances the rate of decarboxylation, as Ruelle et al. (1986) propose. The results of Melius et al. (1990), on the other hand, show that water is also a catalyst for the dehydration path. Their computational study showed that the inclusion of a single water molecule in the transition states for decarboxylation and dehydration reduced the respective energy barriers by roughly equal amounts. Likewise, including a second water molecule in the transition state further reduced the energy barriers, but again by roughly equal amounts. The Melius et al. calculations also showed that the energy barrier for dehydration exceeds that for decarboxylation, in both the absence and presence of water molecules. Therefore, these electronic-structure calculations do not anticipate the experimental observation that CO is the major decomposition product in the gas phase whereas CO_2 is the major product from formic acid decomposition under hydrothermal conditions. This observed inconsistency points out that the quantitative details of the current mechanistic understanding of formic acid decomposition are incomplete and that additional theoretical work is in order. Our efforts in this area are described by Akiya and Savage (1998).

Having proposed a reaction network, we next focus attention on obtaining quantitative estimates for the rate constants for the two parallel reaction paths for formic acid decomposition. These estimates were obtained by fitting the molar yield profiles calculated from numerical solution of the governing differential equations to the experimental data. The differential equations are

$$\frac{d}{d\tau}(MY_{HCOOH}) = -(k_1 + k_2)MY_{HCOOH}$$

$$\frac{d}{d\tau}(MY_{CO_2}) = k_1 MY_{HCOOH}$$

$$\frac{d}{d\tau}(MY_{CO}) = k_2 MY_{HCOOH}$$

where τ is the residence time in the plug-flow reactor and MY_i is the molar yield of compound i. These equations were solved numerically using Euler's method. The objective function that was minimized during the parameter estimation was the sum of the squared differences between the calculated and experimental molar yields of formic acid, CO, and CO_2. This simultaneous differential equation solution and parameter estimation was performed by using the Solver option in a Microsoft Excel spreadsheet. Table 4 displays the estimated first-order rate constants, and Figure 1 compares the calculated and experimental temporal variations of the products' molar yields. It is clear that the use of first-order kinetics for each of the parallel primary paths provides a good quantitative description of these experimental data. The rate constants in Table 4 differ from those in Table 3 because different objective functions were employed in the parameter estimation. The rate constants in Table 3 were calculated by using only the formic acid disappearance data. The rate constants in Table 4, on the other hand, were calculated by using the data for formic acid, CO, and CO_2.

Table 4. First-Order Rate Constants for a Formic Acid Reaction Network

temp (°C)	pressure (atm)	k_1 (1/s)	k_2 (1/s)
320	250	0.053	0.004
340	250	0.093	0.004
360	250	0.070	0.003
380	250	0.143	0.006
420	250	0.470	0.048
380	178	0.296	0.029
380	205	0.352	0.016
380	219	0.459	0.018
380	250	0.107	0.002

Mechanisms

The literature describes several different mechanisms for formic acid decomposition that can potentially occur under the hydrothermal conditions used in the present experiments. As previously discussed, molecular elimination is generally regarded as the most important mechanism for formic acid decomposition in the gas phase (Goddard et al., 1992; Francisco, 1992) and in the presence of water (Ruelle et al., 1986; Melius et al., 1990). Our experimental observations regarding the effect of the water density on the decomposition kinetics and regarding the relative amounts of CO and CO_2 produced, however, are not fully consistent with the quantitative details of the molecular mechanisms proposed in the literature. This inconsistency suggests that either the current concept of the molecular mechanisms is incomplete or some other mechanism might be operative under the hydrothermal conditions of our experiments. Alternative mechanisms include free-radical, ionic, and surface-catalyzed reactions. Each of these mechanistic possibilities is described and discussed in this section.

Free-Radical Reaction. Decomposition of formic acid via free-radical reactions is a possible mechanism under the conditions of our experiments. For example, a reactive COOH radical (or more commonly HOCO) can be formed by removing the hydrogen atom from the C−H bond in formic acid. This formyl C−H bond is weaker than the O−H bond (Singleton et al., 1988). This bond cleavage process could occur through homolytic dissociation or by hydrogen abstraction. The COOH radical can then decompose to form either CO_2 or CO. The set of reactions is as follows.

$$HCOOH = H + COOH$$

$$COOH = H + CO_2$$

$$COOH = OH + CO$$

The H and OH radicals formed in the latter two steps can attack formic acid, abstract hydrogen, and thereby possibly generate additional COOH radicals. Thus, the opportunity might exist for a free-radical chain reaction. Gorden and Ausloos (1961) found it necessary to invoke free-radical chain reactions to explain fully results from the vapor-phase photolysis of formic acid above 200 °C.

The reaction of OH with formic acid has been studied (Singleton et al., 1988; Wine et al., 1985; Jolly et al., 1986), but only near ambient temperature and pressure, which is the region of interest in atmospheric chemistry. Under these conditions, the reaction is complex, and the mechanism has not been established unambiguously. It does appear clear though that OH prefers to attack the O−H bond in formic acid rather than the weaker formyl C−H bond under atmospheric chemistry conditions. At higher temperatures, however, abstraction from the formyl group is expected to make a larger contribution to the overall reaction (Singleton et al., 1988). Nevertheless, a free-radical chain with OH as the chain carrier does not appear to be likely. A chain with H as the chain carrier remains a possibility.

Although a free-radical chain appears to be feasible for formic acid decomposition, it does not appear to be the prevalent mechanism. There is both experimental and computational evidence against a free-radical mechanism being important. Blake and Hinshelwood (1960) found that the addition of propylene and isobutene, which are good free-radical scavengers, had no effect on the rate of formic acid decomposition in the gas phase at temperatures around 500 °C. Hsu et al. (1982) considered the possibility of a radical process for the gas-phase decomposition of formic acid in a shock tube but ruled it out because the kinetics it predicted were not consistent with all of their experimental data. Finally, Goddard et al. (1992) and Francisco (1992) compared the energetics of the molecular mechanisms and the competing free-radical initiation steps and concluded that neither dehydration nor decarboxylation involve free-radical chains.

Ionic Reaction. Because some of the hydrothermal conditions used in the present experiments can support the formation of ions, it is possible that ionic reactions occur during the decomposition of formic acid. For example, formic acid can dissociate according to

$$HCOOH = HCOO^- + H^+$$

and then subsequent decomposition of the anion could produce CO_2. Maiella and Brill (1996) included this type of ionic decomposition mechanism in their analysis of malonic acid decomposition under hydrothermal conditions. They found that only a small amount of the malonate anion was produced (less than 1% yield) and that the rate constant for production of CO_2 from the anion was about 30% lower than the rate constant for production of CO_2 directly from malonic acid. If these results are generally true for other carboxylic acids, one would expect the contribution of ionic reactions to the overall hydrothermal decomposition kinetics of organic acids to be small.

Surface-Catalyzed Reaction. One final potential mechanism that we consider for the decomposition of formic acid under hydrothermal conditions involves surface-catalyzed reactions. There have been numerous studies of formic acid decomposition on the surfaces of well-characterized single crystals at very low pressures, and it is clear that surfaces promote the decomposition. Moreover, surface effects have also been observed or implicated under hydrothermal conditions. For example, Bjerre and Sørensen (1992) obtained different results from formic acid decomposition experiments at 260 °C in new and used reactors. The used reactor led to a higher formic acid conversion, higher yields of CO_2 and H_2, and a lower yield of CO. They attributed the difference to the older reactor surface being rough and corroded. Brill et al. (1996) noted that the temporal variation of the CO_2 profile from formic acid decomposition under hydrothermal conditions was strikingly similar to that observed from decomposition on a Ni(110) surface under ultrahigh-vacuum conditions (Falconer and Madix, 1974). Of course, one must recognize that the reaction conditions are very different in these two studies. One involved pressures of 10^{-7} Torr, whereas the other involved 275 bar.

As noted in a previous section, our experimental results do not show the same behavior as the data reported by Brill et al. (1996). Rather, our data exhibit temporal variations that are consistent with a first-order rate expression, which could describe a homogeneous fluid-phase reaction. Moreover, we did not observe any significant changes in the decomposition kinetics as the reactor S/V ratio was varied.

To summarize this discussion of mechanistic issues and review of the literature, we find that formic acid decomposition under hydrothermal conditions probably proceeds through molecular reaction steps, with the reactions possibly being water catalyzed. Free-radical, ionic, and surface-catalyzed reactions are not expected to be as significant. In closing, we note that the quantitative details of the mechanism for the gas-phase decomposition of formic acid have not yet been fully resolved, so these suggestions regarding the hydrothermal decomposition mechanisms necessarily remain speculative. It is clear that additional experimental work is warranted to resolve issues such as the role of water and metal surfaces in the decomposition reaction.

Summary and Conclusions

Formic acid decomposition under hydrothermal conditions leads to high yields of CO_2 and H_2. The rates of formic acid disappearance and product formation at temperatures above 320 °C are consistent with first-order kinetics. Experiments were conducted to probe the effect of the water density on the decomposition kinetics at 380 °C, but no monotonic trend was apparent. A comparison of the present experimental results with the results one would expect based on the molecular decomposition mechanisms in the literature revealed some inconsistencies in the effect of density on the rate and in the selectivities to CO and CO_2. These inconsistencies lead us to conclude that either physical phenomena are confounding the chemical mechanisms or the quantitative details regarding the mechanism of formic acid decomposition in the presence of water and under hydrothermal conditions have not been fully resolved. Thus, the physical and chemical behavior of this simple organic acid under hydrothermal conditions is both interesting and complex. Additional experimental and computational research that determines the effect of the water density on the kinetics and product yields and that distinguishes between the effects of homogeneous and heterogeneous reactions is warranted.

Acknowledgment

This work was supported, in part, by the National Science Foundation (CTS-9521698, CTS-9311300).

Literature Cited

Akiya, N.; Savage, P. E. The Role of Water in Formic Acid Decomposition. *AIChE J.* **1998** (accepted).

Bjerre, A. B.; Sørensen, E. Thermal Decomposition of Dilute Aqueous Formic Acid Solutions. *Ind. Eng. Chem. Res.* **1992**, *31*, 1574−1577.

Blake, P. G.; Hinshelwood, C. The Homogeneous Decomposition Reactions of Gaseous Formic Acid. *Proc. R. Soc. London, A* **1960**, *255*, 444−455.

Blake, P. G.; Davies, H. H.; Jackson, G. E. Dehydration Mechanisms in the Thermal Decomposition of Gaseous Formic Acid. *J. Chem. Soc. B* **1971**, 1923−1925.

Brill, T. B.; Schoppelrei, J. W.; Maiella, P. G.; Belsky, A. Spectrokinetics of Solvo-Thermal Reactions. *Proc. 2nd Int. Conf. Solvotherm. Reactions*, **1996**, 5−8.

Copa, W. M.; Gitchel, W. B. in *Standard Handbook of Hazardous Waste Treatment and Disposal*; Freeman, H. M., Ed.; McGraw-Hill: New York, 1989; pp 8.77−8.90.

Falconer, J. L.; Madix, R. J. The Kinetics and Mechanism of the Autocatalytic Decomposition of HCOOH on Clean Ni(110). *Surf. Sci.* **1974**, *46*, 473−504.

Francisco, J. S. A Comprehensive Theoretical Examination of Primary Dissociation Pathways of Formic Acid. *J. Chem. Phys.* **1992**, *96*, 1167−1175.

Goddard, J. D.; Yamaguchi, Y.; Schaefer, H. F. The Decarboxylation and Dehydration Reactions of Monomeric Formic Acid. *J. Chem. Phys.* **1992**, *96*, 1158−1166.

Gorden, R.; Ausloos, P. Vapor-Phase Photolysis of Formic Acid. *J. Phys. Chem.* **1961**, *65*, 1033−1037.

Holgate, H. R.; Webley, P. A.; Tester, J. W.; Helling, R. K. Carbon Monoxide Oxidation in Supercritical Water: The Effects of Heat Transfer and the Water−Gas Shift Reaction on Observed Kinetics. *Energy Fuels* **1992**, *6*, 586−597.

Hsu, D. S. Y.; Shaub, W. M.; Blackburn, M.; Lin, M. C. Thermal Decomposition of Formic Acid at High Temperatures in Shock Waves. *Proc. 19th Int. Symp. Combust.* **1982**, 89−96.

Jolly, G. S.; McKenney, D. J.; Singleton, D. L.; Paraskevopoulos, G.; Bossard, A. R. Rate Constant and Mechanism for the Reaction of Hydroxyl Radical with Formic Acid. *J. Phys. Chem.* **1986**, *90*, 6557−6562.

Katritzky, A. R.; Allin, S. M.; Siskin, M. Aquathermolysis: Reactions of Organic Compounds with Superheated Water. *Acc. Chem. Res.* **1996**, *29*, 399−406.

Maiella, P. G.; Brill, T. B. Spectroscopy of Hydrothermal Reactions. 5. Decarboxylation and Kinetics of Malonic Acid and Monosodium Malonate. *J. Phys. Chem.* **1996**, *100*, 14352−14355.

Melius, C. F.; Bergan, N. E.; Shepherd, J. E. Effects of Water on Combustion Kinetics at High Pressure. *Proc. 23rd Int. Symp. Combust.* **1990**, 217−223.

Mishra, V. S.; Mahajuni, V. V.; Joshi, J. B. Wet Air Oxidation. *Ind. Eng. Chem. Res.* **1995**, *34*, 2−48.

Moore, J. W.; Pearson, R. G. *Kinetics and Mechanism*, 3rd ed.; John Wiley & Sons: New York, 1981.

Rice, S. F. Kinetics of Supercritical Water Oxidation. Sandia National Laboratories Combustion Research Facility Quarterly Report (Case 8610.000) for July 1−Sept 30, 1996.

Ruelle, P. Ab Initio Study of the Unimolecular Pyrolysis Mechanisms of Formic Acid: Additional Comments Based on Refined Calculations. *J. Am. Chem. Soc.* **1987**, *109*, 1722−1725.

Ruelle, P.; Kesselring, U. W.; Nam-Tran, H. Ab Initio Quantum-Chemical Study of the Unimolecular Pyrolysis Mechanisms of Formic Acid. *J. Am. Chem. Soc.* **1986**, *108*, 371−375.

Saito, K.; Kakumoto, T.; Kuroda, H.; Torii, S.; Imamura, A. Thermal Unimolecular Decomposition of Formic Acid. *J. Chem. Phys.* **1984**, *80*, 4989−4996.

Savage, P. E.; Gopalan, S.; Mizan, T. I.; Martino, C. J.; Brock, E. E. Reactions at Supercritical Conditions: Fundamentals and Applications. *AIChE J.* **1995**, *41*, 1723−1778.

Singleton, D. L.; Paraskevopoulos, G.; Irwin, R. S.; Jolly, G. S.; McKenney, D. J. Rate and Mechanism of the Reaction of Hydroxyl Radicals with Formic and Deuteriated Formic Acids. *J. Am. Chem. Soc.* **1988**, *110*, 7786−7790.

Thornton, T. D.; Savage, P. E. Phenol Oxidation in Supercritical Water. *J. Supercrit. Fluids* **1990**, *3*, 240−248.

Wightman, T. J. M.S. Thesis, University of California, Berkeley, CA, 1981.

Wine, P. H.; Astalos, R. J.; Mauldin, R. L. Kinetics and Mechanistic Study of the OH + HCOOH Reaction. *J. Phys. Chem.* **1985**, *89*, 2620−2624.

Received for review February 28, 1997
Revised manuscript received October 14, 1997
Accepted October 16, 1997[⊗]

IE970182E

[⊗] Abstract published in *Advance ACS Abstracts*, December 1, 1997.